scientific reports

Check for updates

OPEN

Triple negative breast cancer migration is modified by mitochondrial metabolism alteration induced by natural extracts of *C. spinosa* and *P. alliacea*

Carolina Carlosama, Cindy Arévalo, María Camila Jimenez, Paola Lasso, Claudia Urueña, Susana Fiorentino & Alfonso Barreto✉

Tumor metabolism is a crucial aspect of cancer development, and mitochondria plays a significant role in the aggressiveness and metastasis of tumors. As a result, mitochondria have become a promising therapeutic target in cancer treatment, leading to the development of compounds known as mitocans. In our group, we have consolidated the search of anticancer therapies based on natural products derived from plants, obtaining extracts such as P2Et from *Caesalpinia spinosa* and Anamu-SC from *Petiveria alliacea*, which have been shown to have antitumor activities in different cancer models. These extracts, due to their complex molecular composition, can interfere with multiple functions during tumor progression. To better understand how these natural products operate (P2Et and Anamu-SC), we constructed a model using 4T1 murine breast cancer cells with reduced expression of genes associated with glycolysis (Hexokinase-2) and mitochondrial function (Cqbp). The results indicate that the cells were more sensitive to the Anamu-SC extract, showing significant decreases in glucose consumption, ATP production, and oxygen consumption rate. Additionally, we observed changes in mitochondrial function, which reduced the cells' ability to migrate, particularly when C1qbp was silenced. This triple-negative breast cancer model allows us to identify potential natural products that can modulate tumor cell metabolism.

Keywords TNBC, Metabolism, Plant extracts, Mitocan

The metabolism of tumor cells as a hallmark of cancer was described 100 years ago by Otto Warburg[1], identified an increase in glucose fermentation even in the presence of oxygen, which suggested mitochondrial dysfunction. It is now known that mitochondrial metabolism is essential for the survival and migratory potential of different tumor clones within the tumor[2]. Hanahan and Weinberg listed a series of "cancer hallmarks", among which energy imbalance is one critical point in tumor progression[3,4]. Indeed, tumor cells adapt their energy metabolism to changing conditions, ensuring efficient nutrient use and allowing different metabolic sub-phenotypes to coexist within the same tumor, ultimately promoting growth[5].

Aerobic glycolysis is the predominant metabolism in cells with a high proliferative rate, facilitating the biosynthesis of macromolecules through intermediates like those from the pentose phosphate pathway, which generates nucleotides for DNA synthesis and NADPH for regulating oxidative stress[6]. On the other hand, mitochondrial metabolism through tricarboxylic acid cycle (TCA) and oxidative phosphorylation (OXPHOS), integrating anabolic and catabolic pathways, provides energy support from different energy sources such as glutamine and lipid beta-oxidation, by this means tumor cells can generate amino acids, fatty acids, and nucleotides, allowing

Grupo de Inmunobiología y Biología Celular, Unidad de Investigación en Ciencias Biomédicas, Facultad de Ciencias, Pontificia Universidad Javeriana, Carrera 7a. No. 43-82, Ed. 50, Lab. 101, 110211 Bogotá, Colombia. ✉email: alfonso.barreto@javeriana.edu.co

the production of metabolites as intermediary substrates. In this sense, OXPHOS supports progression and metastasis in different cancer models[5,7,8].

Hexokinase, a key enzyme in glycolysis, phosphorylates glucose to form glucose 6-phosphate (G6P), marking an essential and irreversible step in metabolism[8]. The expression of hexokinase isoform 2 (Hk-2) expression rises during tumor formation, enhancing glucose absorption and providing the cell with energy and access to many intermediary substrates for proliferation. Hence, inhibition of glucose uptake by pharmacological mechanisms such as 2-deoxyglucose (2-DG) or RNA interference induced a reversal of tumorigenesis, leading to a compensatory increment of OXPHOS metabolism[9,10]. Additionally, the C1qbp (P32) protein, which regulates mitochondrial function[11] participates in the process of mitochondrial biogenesis and is reported as overregulated indifferent types of cancer; supports OXPHOS by interacting with the pyruvate dehydrogenase (PDH) enzyme. Inhibiting C1qbp leads to metabolic shifts that increase glycolysis while decreasing OXPHOS in various cell models[11,12].

Triple-negative breast cancer (TNBC) exhibits a heterogeneous metabolic phenotype with an exacerbated glycolytic metabolism due in part to an increased expression of glycolysis-associated receptors and enzymes such as GLUT1, HK-2, and LDH, among others. There are numerous metabolic pathway-based subtypes with varying sensitivities to drugs that function as metabolic inhibitors; each also has a unique clinical outcome, with the high glycolytic subtype tumor having the poorest prognosis[13–16]. The treatment of TNBC depends on the molecular subtype, and the most common therapies include surgery, radiation therapy, and chemotherapy, with taxanes and anthracyclines being the most used[17]. Nevertheless, relapse and poor prognosis remain the Achilles heel in this type of tumor and have become a challenge in drug discovery[18].

The search for new drugs that target the metabolism has increased in recent years, and among these, various plant extracts have been shown to influence different metabolic pathways[19–21]. Natural compounds potentially operate as enzyme inhibitors, directly targeting the enzyme's function or impacting genes and oncogenes involved in the glycolytic system[22]. Flavonoids like curcumin, resveratrol, quercetin, and EGCG can reduce the expression of glycolytic enzymes in various tumor models[19–21,23]. On the other hand, natural products can also target mitochondrial functions, including the TCA cycle, ETC, and OXPHOS, making them potential "mitocans", for cancer treatment. This mitocans are described as a collection of compounds that demonstrate anti-cancer effects through their interactions with molecular targets in mitochondria[24–28]. Terpenoids from various plants, such as *Bombax ceiba*, *Gardenia jasminoides*, *Alisma orientale*, or fruits, such as grapes and red fruits, are some of these natural products that can alter mitochondrial function and have an anti-tumor effect. Other natural products that can do the same include types of flavonoids and saponins[24,29]. In TNBC, the OXPHOS pathway is overactivated, and its dysfunction impacts cancer cell motility and increases chemotherapy sensitivity[29–31].

We have previously obtained and described a flavonoid-rich extract called P2Et obtained from the plant *C. spinosa*, which showed cytotoxic activity accompanied by an alteration in mitochondrial membrane potential, an increase in cytoplasmic calcium levels, damage-associated molecular pattern molecules (DAMPs) exposure in the cell surface, and induction of immunogenic cell death[32,33]. Similarly, from *P. alliacea*, we obtained the extract Anamu-SC, rich in flavonoids and sulfur compounds[34]. Treatment in 4T1-tumor cells showed a metabolic modulating effect with decreased glycolytic activity and decreased expression of the mitochondrial complex V in a triple-negative breast cancer[35,36]. In this context, we wanted to delve into the impact of each of these extracts and enhance our understanding of the biological function of polymolecular drugs, particularly regarding the participation of cell metabolism in controlling tumor cell death or migration. To accomplish this, we generated clones of the mouse breast cancer cell line 4T1 with a diminished expression of either the hexokinase-2 enzyme or C1qbp, showing alterations in glycolysis or OXPHOS, respectively. We assessed the relationship between these metabolic phenotypes in response to therapy with these natural extracts.

Methods

Plant material and natural extracts production

Leaves and stems from *Petiveria alliacea* L., Phytolaccaceae (local name "anamu") were collected in Cachipay, Cundinamarca, Colombia and identified by Antonio Luis Mejia from the Colombian National Herbarium; voucher number COL 569,765 (Colombian Environmental Ministry agreement number 1927 related to these of genetic resources and derivatives products). *P. alliacea* extraction procedure and chemical characterization were previously described[37,38].

Caesalpinia spinosa (Molina) Kuntze pods were collected in Villa de Leyva, Boyacá, Colombia. Plant material was identified by Luis Carlos Jimenez, from the Colombian National Herbarium (voucher specimen number COL 523,714. Colombian Environmental Ministry agreement number 220/2018 related to the use of genetic resources and derived products). The P2Et extract was produced under GMP conditions and chemically characterized as previously described[39,40]. In each assay, P2Et was diluted in 95% ethanol, obtaining a 25 mg/mL fresh solution.

Cell line and culture conditions

The 4T1 wild-type (WT) murine mammary carcinoma cell line (ATCC-CRL-2529) was originally provided by Dr. Alexzander Asea from Texas A&M Health Science Center College of Medicine in Temple, TX[37,41]. In the laboratory, the cell line was initially activated by inoculation into Balb/c mice, then recovered and cultured, and used between passage 3 and 10 for the experiments in the article. This cell line served as the parental line for the derivative clones 4T1-F10 (sh-Hk2)9 and 4T1-C12 (sh-C1qbp)11. The cells were cultured in RPMI-1640 (Gibco, Waltham, MA, USA) enriched with; penicillin (100 U/mL), HEPES buffer (0.01 M), L-glutamine (2 mM), sodium pyruvate (1 mM) and streptomycin (100 µg/mL) (Gibco, Waltham, MA, USA) including 10% heat-inactivated fetal bovine serum (FBS) (Eurobio, Les Ulis, France). The cultures were maintained in a humidified atmosphere at 37 °C with 5% CO_2. Cells were allowed to grow to approximately 80% confluence before passaging using

trypsin–EDTA. Additionally, the 4T1-F10 and 4T1-C12 cells were maintained with 10 µg/mL of puromycin (Gibco, Waltham, MA, USA).

HK-2 and C1qbp shRNA knockdown

The shRNA lentiviral particles targeting *Hexokinase 2* (sc-35622-V), and *C1qbp* (sc-42881-V) were purchased from Santa Cruz Biotechnology (Santa Cruz, CA USA). 2.5×10^4 4T1 cells seeded on 48 well plate were transduced with 10^6 virus particles in RPMI-1640 (Eurobio) supplemented with 10% FBS (Eurobio), 2 mM L-glutamine, 100 U/mL penicillin, 100 µg/mL streptomycin, 0.01 M HEPES buffer, and 1 mM sodium pyruvate (Eurobio, Les Ulis Cedex B, France). Then, 5 µg/mL of polybrene was added and transduction was done in a humidified environment at 37 °C and 5% CO_2 following the manufacturer's instructions. Fresh medium was added every other day and cells were cultured in the presence of 10 µg/mL puromycin to select resistant cells (Gibco, Waltham, MA, USA). After 90% cell confluence, cells were trypsinized, expanded, and a monoclonal cell population was obtained throughout limiting dilution. After expanding different clones, the efficacy of the lentivirus-mediated shRNA knockdown of Hk-2 and C1qbp was confirmed by *Western blot.*

HK-2 and C1qbp expression analysis by western blotting

Cells were trypsinized, washed twice with PBS and lysed on ice for 20 min with RIPA buffer (150 mM NaCl, 50 mM Tris–HCl, pH 7.4, 1 mM EDTA, 1% Triton X-100, 0.1% SDS, 0.5% sodium deoxycholate). Lysates were centrifuged, and protein concentration was measured using the Pierce BCA Protein Assay Kit according to the manufacturer's instructions (Thermo Scientific, Massachusetts, USA). A total of 20 µg of protein were separated on a 10% SDS-PAGE and transferred to polyvinylidene fluoride (PVDF) membranes. Membranes were blocked in (Tris-buffered saline with 0.1% Tween® 20 detergent) TBST-T supplemented with 5% nonfat dry milk for 1 h at room temperature. The primary antibodies rabbit mAb anti-hexokinase II (C64G5, Cell Signaling, Massachusetts, USA), rabbit mAB anti-C1qbp (D7H12, Cell Signaling, Massachusetts, USA) and monoclonal mouse IgG1 anti-β-actin antibody (MAB8929 from R&D systems, Minneapolis, USA) were incubated overnight at 4 °C, followed by specific secondary antibody, goat anti-rabbit IgG (H + L) secondary antibody HRP-conjugated (Novus, USA) and goat anti-mouse IgG antibody (H + L) HRP conjugate (Merck, Darmstadt, Germany). Membrane-bound immune complexes were visualized using SuperSignal West Pico chemiluminescent substrate (Pierce, Rockford, IL, USA) in an iBright FL1500 imaging system (Thermo-Fisher, Massachusetts, USA).

OCR and ECAR evaluation

The oxygen consumption rate (OCR) and extracellular acidification rate (ECAR) were measured using the Agilent MitoXpress and pH-Xtra assays, respectively, following the manufacturer's protocols[46–48] as was described before[49]. In this study, 4T1-WT, 4T1-F10, and 4T1-C12 cells were plated in a 96-well format at a density of 3.0×10^4 cells per well and treated for 6 h with the IC_{50} concentrations of P2Et or Anamu-SC as indicated by the MTT assay results (Fig. 5A). The controls of this type of experiments were added before the measure in the Cytation5 Reader (BioTek, Winooski, VT, USA). In this order, the OCR control was 1 µM AntiA (Antimycin A from *Streptomyces sp*, Sigma-Aldrich, Massachusetts, USA); and for the ECAR was used 50 mM 2-DG (2-deoxy-D-glucose, > 98%, Sigma-Aldrich, Massachusetts, USA). Afterwards, the measure of fluorescence decay rate was made it as the manufacturer's protocol using the formula: Lifetime (µs)[τ] = (D2 – D1)/ln(IW1/IW2). The values of IW1 and IW2 are the two measurement windows; and D1 and D2 are the delay times before having the values of W1 and W2.

Glucose uptake assay

The glucose uptake assay was conducted using the fluorescent glucose analog 2-NBDG (2-(N-(7-Nitrobenz-2-oxa-1,3-diazol-4-yl)Amino)-2-Deoxyglucose) (Invitrogen™/Molecular Probes, Carlsbad, CA, USA) and analyzed by flow cytometry[50,51] and described previously[42]. The procedure was as follows; 1×10^5 4T1-WT, 4T1-F10, and 4T1-C12 cells were plated in 12-well plates and incubated overnight. Then, the cells were treated for 24 h with the IC_{50} concentration of P2Et, the IC_{50} and $IC_{50/5}$ concentrations of Anamu-SC, 100 nM ascorbic acid (as an antioxidant control), 1 µM rotenone (a mitochondrial inhibitor), and either H_2O or ethanol (as negative controls at 0.02%). To continue the cells were first stained with LIVE/DEAD fixable aqua kit to identify viable cells; subsequently, cells were incubated with 25 µM 2-NBDG in PBS for 30 min at 37 °C. After washing and resuspension in PBS, samples were analyzed using a Cytek Aurora flow cytometer (Cytek Biosciences, Fremont, CA, USA). FlowJo software v10.8.1 software (BD Life Sciences, New Jersey, USA) was used to analyze the flow cytometry data. Experiments were performed in duplicate on three independent experiments and the results were expressed as mean ± SEM.

ROS measurement

To evaluate ROS production, a total of 1×10^5 4T1WT, 4T1-F10 and 4T1-C12 cells were seeded on 12-well plates and incubated overnight. Then cells were treated with the IC_{50} of the P2Et, the IC_{50} and $IC_{50/5}$ of Anamu-SC; 100 nM Ascorbic acid, 1 µM rotenone and H_2O or ethanol (negative controls, 0.02%) for 24 hours. Then cells were labelled with 1 µM 2′,7′ dichlorodihydrofluorescein diacetate (H_2DCFDA) (Sigma Aldrich, Massachusetts, USA) for 40 min at 37 °C followed by propidium iodide (PI) (Sigma-Aldrich, Massachusetts, USA) or 1 µM MitoSOX™ Red Mitochondrial Superoxide (Molecular Probes, Invitrogen Corp, Carlsbad, CA, USA) for 30 min at 37 °C. Each sample was then acquired using an FACSAria II-U flow cytometer (BD, Biosciences, San Jose, USA) for H_2DCFDA and Cytek Aurora flow cytometer (Cytek) for MitoSOX. Data were analyzed with FlowJo v10.8.1 software (BD Life Sciences). Experiments were performed in duplicate on three independent experiments and the results were expressed as mean ± SEM.

ATP determination

The intracellular ATP analysis was performed using the ATP Bioluminescence Assay Kit HS II from Roche, following the manufacturer's protocol explained before[33,49]. The experimental procedure was as follows: 1×10^5 cells of 4T1-WT, 4T1-F10, and 4T1-C12 were plated in 12-well plates and incubated overnight. The cells were then treated for 24 h with the IC_{50} concentration of P2Et, the IC_{50} and $IC_{50/5}$ concentrations of Anamu-SC, 100 nM ascorbic acid, 1 µM rotenone and either H_2O or ethanol (as negative controls at 0.02%). Following, the signal was capture in the Cytation5 Reader (BioTek, Winooski, VT, USA). The experiments were conducted in duplicate across three independent trials, and the results were reported as mean ± SEM.

Growth rate assay

4T1-WT, 4T1-F10, and 4T1-C12 cells were plated in 12-well plates at a density of 4000 cells per cm^2. After 24, 48, and 72 h, the cells were harvested and counted using 0.4% trypan blue. The population doubling time (PDT) was determined using the exponential growth method (Malthusian) through GraphPad Prism version 8.1.1 for Mac OS X statistics software (GraphPad Software, San Diego, CA) described before[49].

In vitro cytotoxicity assay

The methylthiazol tetrazolium (MTT) assay (Sigma-Aldrich, Massachusetts, USA) was utilized to assess the viability of tumor cells treated with plant extracts and doxorubicin detailed previously[37,40]. For each experiment, 4×10^3 cells were plated in 96-well plates. Treatments were given for 48 h in serial dilutions, starting from 250 µg/mL and decreasing to 0.97 µg/mL. After the treatment period, 100 µL of non-phenol red media and 50 µL of 1X MTT were added to each well, followed by a 4-h incubation at 37 °C. Subsequently, 100 µL of DMSO was added to dissolve the formazan crystals, and the plates were incubated for an additional 20 min. The absorbance was then measured at 540 nm using a Multiskan™ FC Microplate Photometer (Thermo Scientific, Massachusetts, USA). The IC_{50} values (50% inhibition of cell growth) were calculated using GraphPad Prism version 8.1.1 for Mac OS X, employing a non-linear regression log (inhibitor) versus response-variable slope formula. Experiments were conducted in triplicate across three independent trials, with results expressed as mean ± SEM.

Annexin V and PI double-staining assay

Phosphatidylserine (PS) externalization was assessed using flow cytometry with Annexin V-FITC (Molecular Probes, Invitrogen Corp, Carlsbad, CA, USA) and propidium iodide (PI) (Sigma-Aldrich, Massachusetts, USA) staining[54,55] and analyzed by flow cytometry following the previously mentioned protocol[40]. The protocol involved seeding 1×10^5 cells (4T1-WT, 4T1-F10, and 4T1-C12) in 12-well plates and incubating them overnight. Cells were then treated for 24 h with various compounds, including IC_{50} of P2Et, IC_{50} and $IC_{50/5}$ of Anamu-SC, 100 nM ascorbic acid, 1 µM rotenone, and controls (H_2O or 0.02% ethanol). After treatment, cells were harvested and resuspended in annexin buffer (100 mM HEPES, 140 mM NaCl, 2.5 mM $CaCl_2$)[55]. The cell suspension was incubated with Annexin V-FITC for 8 min at room temperature, followed by a 3 min incubation with PI at 4 °C. Data acquisition was performed using a FACSAria II-U flow cytometer, and the results were analyzed using FlowJo v10.8.1 software.

Mitochondria membrane potential (MMP) assay

To evaluate MMP, 1×10^5 4T1-WT, 4T1-F10 and 4T1-C12 cells were seeded on 12-well plates and incubated overnight. Then cells were treated for 24 h with the IC_{50} of the P2Et, the IC_{50} and $IC_{50/5}$ of Anamu-SC; 100 nM Ascorbic acid (anti-oxidant), 1 µM rotenone (mitocan), valinomycin (positive control, 0.1 µg/mL) and H_2O, or ethanol (negative controls, 0.02%) for 24 h. MMP was measured using JC-1 (Sigma-Aldrich, Massachusetts, USA) dye. The cells were acquired on a FACSAria I (Becton, Dickinson and Company, New Jersey, USA) and analyzed with FlowJo software (Tree Star Inc., Ashland, OR), which calculated the red/green fluorescence ratios. Duplicate estimations were made, and the average was expressed as mean ± SEM in three independent experiments.

Mitochondrial density and morphological analysis

For mitochondrial density, 1×10^5 4T1-WT, 4T1-F10 and 4T1-C12 cells were seeded on 12-well plates and incubated overnight. Then cells were stained with 0.2 µM of MitoTracker Red CMXRos (Molecular Probes, Invitrogen Corp, Carlsbad, CA, USA) for 30 min at 37 °C. Each sample then was acquired using a Cytek Aurora flow cytometer (Cytek Biosciences). The samples were analyzed with FlowJo v10.8.1 software (BD Life Sciences). Experiments were performed in triplicate and the results were expressed as mean ± SEM.

Mitochondria morphological parameters were evaluated by immunofluorescent microscopy. 2×10^4 4T1-WT, 4T1-F10, and 4T1-C12 cells were seeded on a 35 mm glass bottom dish with 10 mm micro-well treated with 0.1% fibronectin and were grown overnight in 1 mL of RPMI-1640 medium. Subsequently, they were treated for 24 h with IC_{50} of Anamu-SC: 125 µg/mL for 4T1-WT, 121.6 µg/mL for 4T1-F10 and 60.39 µg/mL for 4T1-C12 and 1 µM rotenone for 5 min. At the end of time, cells were fixed with 4% paraformaldehyde and 0.1% glutaraldehyde for 20 min, then washed and permeabilized with 0.1% Triton X-100 for 10 min. Next, blocking was carried out with 50 mM NH_4Cl for 10 min, followed by incubation with MitoTracker™ Red CMXRos (Molecular Probes, Invitrogen Corp, Carlsbad, CA, USA) for 20 min at 37 °C. Finally, cells were stained with 300 nM DAPI (Molecular Probes, Invitrogen Corp, Carlsbad, CA, USA) for 5 min. Images were acquired with an Olympus FV1000 confocal microscope, with a 60 × PlanAPO oil objective. Quantitative mitochondrial analysis was performed on 50 cells per coverslip according to the protocol described by Koopman et al.[56] and Tronstad et al.[57] using ImageJ software 1.52 q. Parameters calculated from the images for each condition were: the number of mitochondrial objects per cell (Nc), the mean area of each individual mitochondrial object (Am), mitochondrial mass (the

product of Nc and Am), the mean mitochondrial object aspect ratio (AR, a measure of mitochondrial length), and the mean mitochondrial object shape/form factor (FF, a combined measure of mitochondrial length and degree of branching).

Wound healing assay

To assess cell migration, a scratch wound assay was performed using a standard pipette tip to create gaps in the cell monolayer[58,59]. The experiment also described before[43] utilized 4T1-WT, 4T1-F10, and 4T1-C12 cells, which were initially seeded at a density of 1×10^5 cells per well in 12-well plates and allowed to adhere overnight. The cells were then exposed to $IC_{50/5}$ concentrations of P2Et and Anamu-SC treatments. Following a 48-h incubation period in RPMI-1640 supplemented medium, the cells were re-seeded in 12-well plates and cultured until they formed a confluent monolayer (approximately 90% confluence). Once confluence was achieved, the cell monolayer was wounded by scratching with a pipette tip, creating a cell-free area. The wounded monolayers were then cultured in fresh Opti-MEM I Reduced Serum Media. To monitor wound closure, images were captured at the initial time point and at 12- and 24-h post-wounding[43]. The cell migration was documented using a low magnification (4×) objective on a BioTek Cytation 5 Cell Imaging Multimode Reader (BioTek, Winooski, VT, USA). Quantitative analysis of wound size measurements was performed using ImageJ software, a widely used tool for such analyses.

qPCR of EMT transcription factors

The TRIzol LS reagent (Life Technologies Corporation, Invitrogen, NY) was used to have the total RNA from 4T1-WT, 4T1-F10, and 4T1-C12 cells according to the manufacturer's protocol and previously described[43]. The process began by seeding 1×10^5 cells overnight, followed by resuspension in TRIzol. cDNA synthesis was performed using SuperScript III Reverse Transcriptase (Invitrogen) as per the manufacturer's guidelines. RNA quality and quantity were evaluated using a NanoDrop spectrophotometer (NanoDrop Technologies). For real-time PCR, reactions were set up in a total volume of 20 µL, containing 600 ng of cDNA, iTaq Universal SYBR Green Supermix (BIORAD, CA, USA), and 250 nM of both forward and reverse primers. To assess the expression of Snail, Twist, and Zeb genes, the following specific primers were utilized (Table 1):

Data was collected from two independent experiments, each performed in duplicate, using the QuantStudio™ 3 Real-Time PCR System (Molecular Probes, Invitrogen Corp, Carlsbad, CA, USA). The PCR thermal cycling program consisted of an initial denaturation step at 95 °C for 30 s, followed by 40 cycles of denaturation at 95 °C for 15 s; annealing at the appropriate temperature for 60 s and extension at 72 °C for 40 s, finally, the program concluded with a dissociation phase to verify amplification specificity.

Gene expression levels were normalized to the housekeeping gene GAPDH, which served as an endogenous control. Relative expression was then calculated using the 2^(− ΔΔCT) comparative method, allowing for quantitative comparison of gene expression across different samples and conditions.

Statistical analysis

For statistical analysis we employed between two groups was calculated using the Mann–Whitney U test, while differences among groups were calculated using Kruskal–Wallis and Dunn's posttest for multiple comparisons. GraphPad Prism version 8.1.1 for Mac OS X statistics software (GraphPad Software) was used.

Results

Hk-2 downregulation in 4T1 cells reduces glucose uptake, ATP, and ROS production

We generated two stable clones with different metabolic characteristics through the knockdown of the Hk-2 and the C1qbp proteins in the murine breast cancer 4T1 cells transducing lentiviral particles containing three shRNA in a puromycin resistance vector. Thus, after transduction, we selected by limiting dilution and obtained the stable clones for each single protein: 4T1-F10 and 4T1-C12 clones for *Hk-2* and *C1qbp* downregulation, respectively. Western blot analysis of the expression levels of Hk-2 in the F10 clone and C1qbp in the C12 clone confirmed that each protein's expression was diminished by the shRNAs (Fig. 1A). Then, we examined glucose uptake, intracellular ATP production, mitochondrial mass, and intracellular/mitochondrial reactive oxygen species (ROS/mtROS). In the 4T1-F10 clone compared to the 4T1-WT, we observed a decreased glucose consumption, ATP generation, and mtROS with a tendency to increase mitochondrial mass (Fig. 1B–F). However, compared to 4T1-WT cells, the 4T1-C12 clone only showed a decrease in ATP generation; this could be because 4T1-WT cells have a high rate of glycolysis[61].

Primer name	Sequence
Snail1	Forward: CTCTGAAGATGCACATCCGAA
	Reverse: GGCTTCTCACCAGTGTGGGT
Twist1	Forward: GCCGGAGACCTAGATGTCATTG
	Reverse: CACGCCCTGATTCTTGTGAA
Zeb1	Forward: GCCAGCAGTCATGATGAAAA
	Reverse: TATCACAATACGGGCAGGTG

Table 1. Primers sequences used to evaluate expression of *Snail, Twist and Zeb* genes.

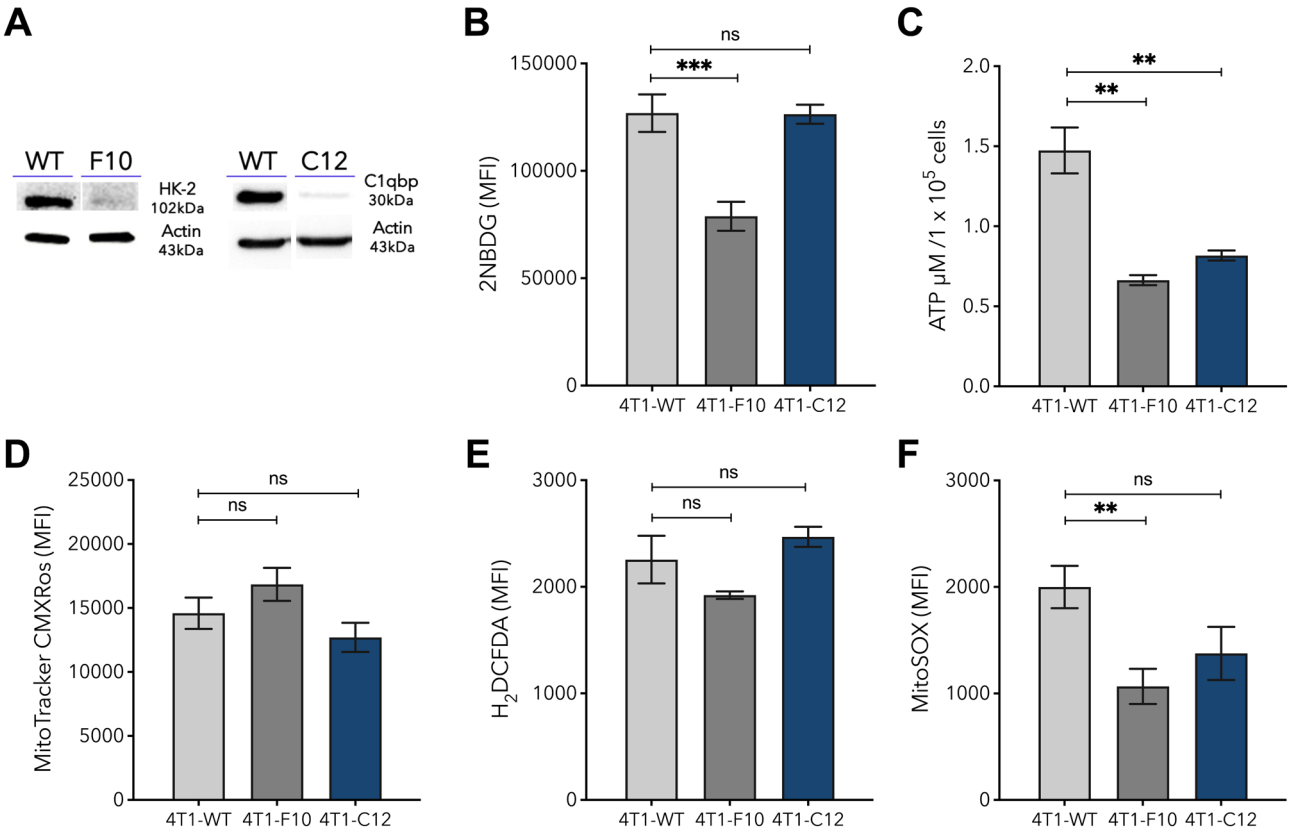

Fig. 1. Metabolic parameters evaluation in shRNA-Hk-2 and shRNNA-C1qbp 4T1 clones. (**A**) Western blotting showing protein Hk-2 and C1qbp expression of each clone, 4T1-F10 (*Hk-2*) and 4T1-C12 (*C1qbp*). (**B**) 4T1-WT, 4T1-F10 and 4T1-C12 clones were seeded and after 24 h were stained with 2-NBDG dye showing MFI (median fluorescence intensity). (**C**) 4T1-WT, 4T1-F10 and 4T1-C12 cell were seeded overnight then cells were lysed and supernatant recollected showing bioluminescence per 100.000 cells. (**D**–**F**) 4T1-WT, 4T1-F10 and 4T1-C12 cells were seeded overnight and then, stained with mitotracker CMXRos (**D**), H_2DCFDA (**E**), and MitoSOX (**F**), figures showed MFI of each probe. Data are presented as the mean ± SEM of three independent experiments $^{*}p<0.05$; $^{**}p<0.01$; $^{***}p<0.001$; $^{****}p<0.0001$.

Hk-2 and *C1qbp* downregulation in 4T1 cells modulate glycolysis and OXPHOS metabolism

Then, we looked for variations in the ECAR and OCR between 4T1-WT cells and their clones. We found that only the 4T1-F10 clone significantly increased the OCR compared to 4T1-WT cells, whereas the ECAR significantly decreased in both clones (Fig. 2A). The response of 4T1-WT and its clones to the glycolysis inhibitor 2DG and the inhibitor of the mitochondrial electron transport chain, antimycin, was then assessed in ECAR and OCR, respectively. We observed that clone 4T1-F10, were sensitive to 2DG, lowering ECAR, and that both clones 4T1-1-F10 and 4T1-C12 lowered OCR in response to antimycin (Fig. 2B). The ECAR/OCR rate analysis showed that 4T1-WT and 4T1-C12 preferentially use glycolysis, while 4T1-F10 uses OXPHOS, suggesting that clone 4T1-F10 has a marked tendency to use this pathway, in fact, this clone showed a lower glucose consumption (Fig. 1B), as expected, whereas the 4T1-C12 clone was similar to 4T1-WT cells being more glycolytic (Fig. 2C)[9,11]. Besides, plotting OCR vs ECAR results we could separate the cells into different metabolic phenotypes (Fig. 2D) as previously shown in other models[62]. These findings demonstrate that, in this TNBC cell model, metabolic regulation via Hk-2 knockdown may rely to an OXPHOS-depending metabolic model, whereas C1qbp inhibition does not clearly distinguish itself from 4T1-WT cells.

Hk-2 and C1qbp downregulation in 4T1 cells increase cellular migration

The alteration of different metabolic pathways at the tumor cell level is related to changes in proliferation index and cell migration[63–65]. To confirm this response, first, we wanted to compare the growth rate between the 4T1-WT cells and the clones through the measurement of the population doubling time (PDT). The 4T1-F10 clone proliferated at a slower rate than WT cells, while there were no alterations in the 4T1-C12 clone (Fig. 3A). Next, using the wound closure assay, we observed that both clones had a higher percentage of wound closure compared to WT cells, with no differences in the migration between the clones (Fig. 3B). Since tumor cell migration is related to changes in the epithelial-mesenchymal transition (EMT), a set of transcription factors associated with it were evaluated (Table 1). We found a significant increase in *Zeb1* relative expression in the 4T1-C12 clone. Still, no variation was found between the WT cells and the 4T1-F10 clone (Fig. 3C). These results suggest that

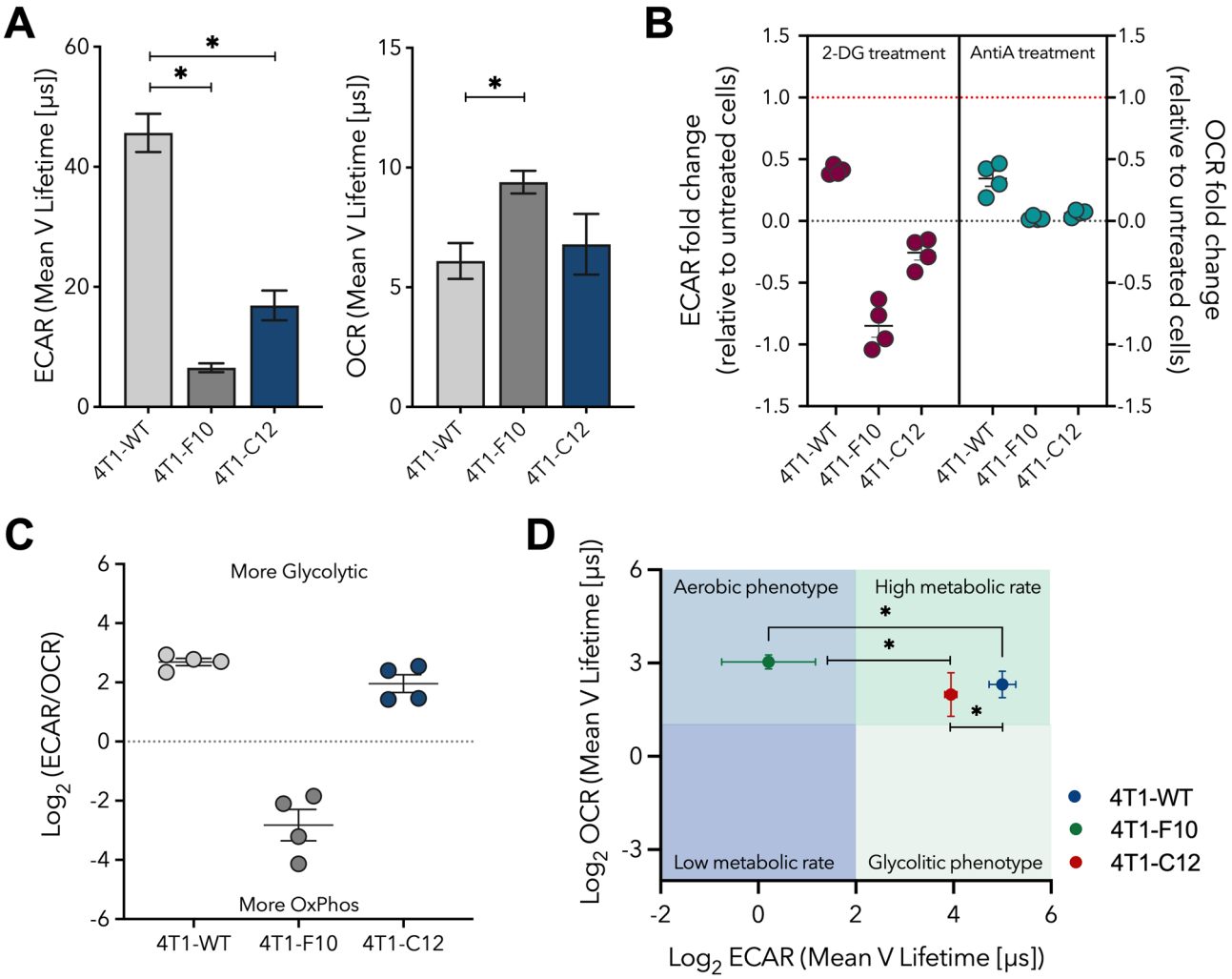

Fig. 2. ECAR and OCR differences in 4T1-WT, *Hk-2* and C1qbp knockdown cells. (**A**–**D**) Cells were seeded in 96-well plate overnight, and next day cells were stained with MitoXpress probe, or pH-Xtra Glycolysis probe and oxygen consumption rate (OCR) and extracellular acidification rate (ECAR) were measured. (**A**) ECAR and OCR basal measurement in 4T1-WT, 4T1-F10 and 4T1-C12. (**B**) Graph shows in Y left axis the ECAR fold change (dot red line) with the 2-DG 50 mM (glycolysis inhibitor) and Y right axis shows the OCR fold change (dot red line) with antimycin A 1 µM electron transport chain (ETC) inhibitor. (**C**) Graph shows the ratio between ECAR and OCR in the different cells. (**D**) Graph shows the metabolic profile of cells. Data are presented as the mean ± SEM of 3 independent experiments $^{*}p<0.05$; $^{**}p<0.01$; $^{***}p<0.001$; $^{****}p<0.0001$.

the ability to migrate is related to metabolic modulation, which may involve pathways other than the activation of EMT transcription factors.

Changes in mitochondrial function reduce the migration ability of 4T1-F10 and 4T1-C12

Mitochondria may be a therapeutic target for a group of drugs known as mitocans[25,26], including substances such as rotenone that inhibit mitochondrial complex I[66]. Thus, we studied the effect of rotenone in the mitochondria membrane potential (MMP) on 4T1-WT cells and its derived clones. Rotenone treatment increased MMP loss in WT and clones, with the *C1qbp* knockdown clone being less sensitive, while the Hk-2 inhibition clone had the greatest loss, likely due to a reduction in glucose consumption (Fig. 4A). Then, after rotenone treatment, we measured ROS/mtROS from the cells and discovered an increase in both parameters in all cells, with mtROS being higher in WT cells (Fig. 4B). However, analysis of cell migration revealed a decrease in both clones, with clone C12 showing a higher decline. Since WT cells did not form a confluent cell monolayer in the wound healing assay after being treated with rotenone (Fig. 4C), the assay could not be carried out on them. Then, we wanted to see if the effect of rotenone on migration was connected to a metabolic aspect such as ATP production, and we discovered a significant reduction 24 h after treatment in 4T1WT cells and both clones (Fig. 4D). These findings suggest that mitocans therapy impairs mitochondrial function independent of metabolic fitness, and that this impairing affects tumor cell migration.

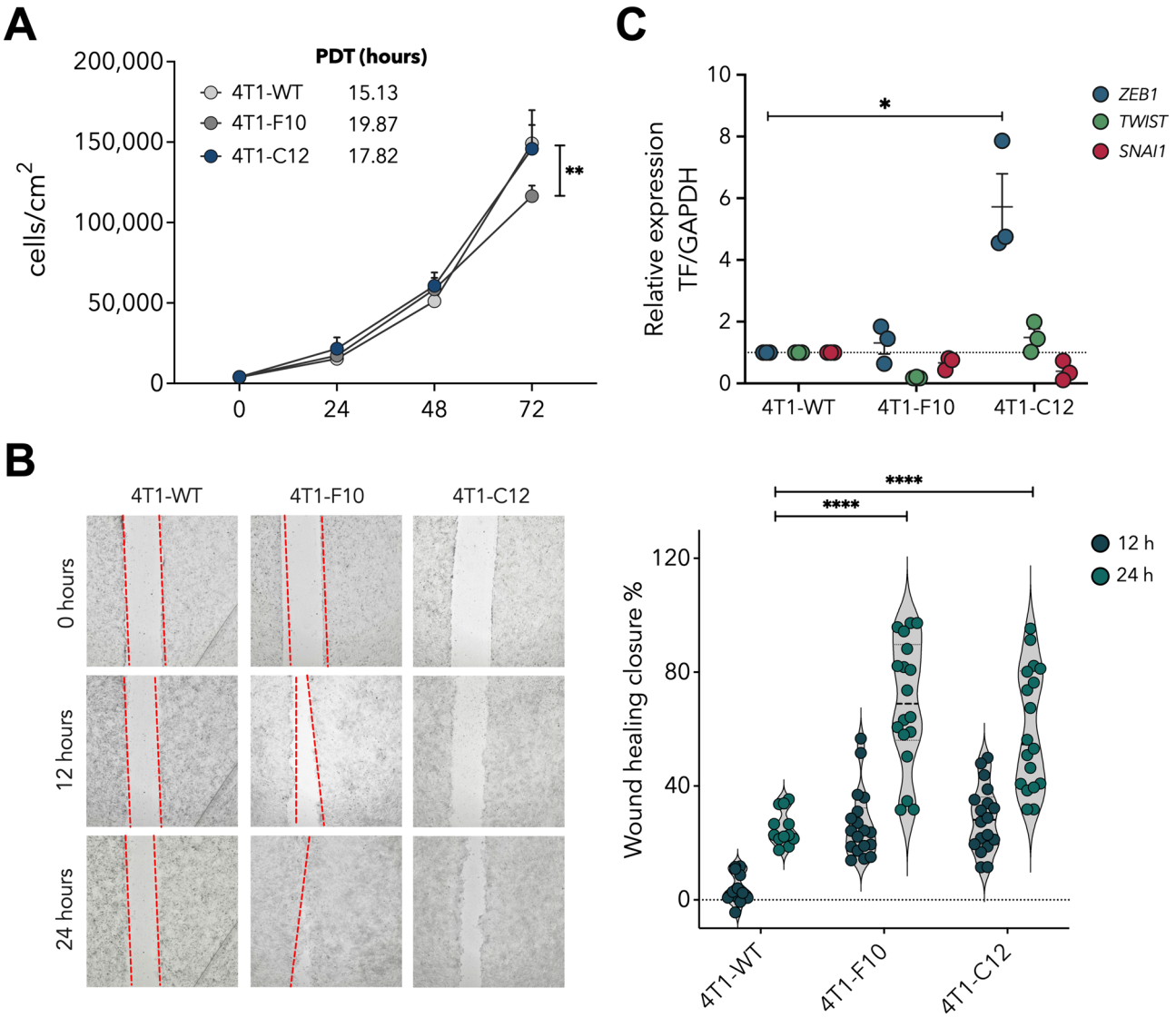

Fig. 3. Migration in 4T1 cells with deficit in *Hk-2* and *C1qbp*. (**A**) Growth curve of 4T1-WT, 4T1-F10 and 4T1-C12 clones seeding at density of 4000 cells/cm^2. Data are presented as mean ± SEM. (**B**) Cell migration images (wound healing assay) of 4T1-WT, 4T1-F10 and 4T1-C12 cells showed an increase in wound closure of the clones over WT cells with graph representation of percentage closure at 12 h and 24 h in 4T1WT cells and their clones. (**C**) Relative expression of the EMT transcription factors *Zeb, Twist* and *Snail* in 4T1WT cells and their clones, analyzed by the $2^{-\Delta\Delta Ct}$ method compared with 4T1WT cells as control (red dash line). Data are shown as mean ± SEM $^*p<0.05$; $^{**}p<0.01$; $^{***}p<0.001$; $^{****}p<0.0001$.

Anamu-SC reduced the 4T1-F10 and 4T1-C12 tumor cells migratory potential and altered tumor mitochondrial metabolism

To investigate whether natural extracts with antitumor activity exerted their function through the regulation of mitochondrial function, we evaluated the effect of P2Et and Anamu-SC on the mitochondrial-related biological functions: glucose consumption, ATP, and ROS production. First, we found that the 4T1-F10 clone presented with ten times more sensitivity to cell death when treated with Anamu-SC compared to 4T1-WT, and two times more than the 4T1-C12 clone. No differences were observed between WT cells and the clones in terms of their sensitivity to the P2Et extract (Fig. 5A). Therefore, in the following tests the IC_{50} of the extracts were calculated for each clone. We observed that Anamu-SC caused a decrease in glucose uptake in 4T1-WT cells and the 4T1-C12 clone. Still, it did not affect the 4T1-F10 clone, probably due to the inhibition in Hk-2 (Fig. 5B). In addition, and as it was expected, the Anamu-SC as well as the rotenone treatment caused a reduction in ATP production in the WT cells and clones[35]. On the other hand, the P2Et extract did not influence ATP production in the clones, but it did decrease ATP production in WT cells (Fig. 5C).

We performed a parallel analysis of ROS and mtROS production, expecting that Anamu-SC treatment would cause an increase in ROS due to mitochondrial impairment. Indeed, we found an increase in both parameters in all cells, with more mtROS production in the WT cells (Fig. 5D). Then, using the IC_{50} of P2Et and Anamu-SC, we evaluated the OCR and ECAR after 6 h of treatment. P2Et treatment did not produce any differences, while

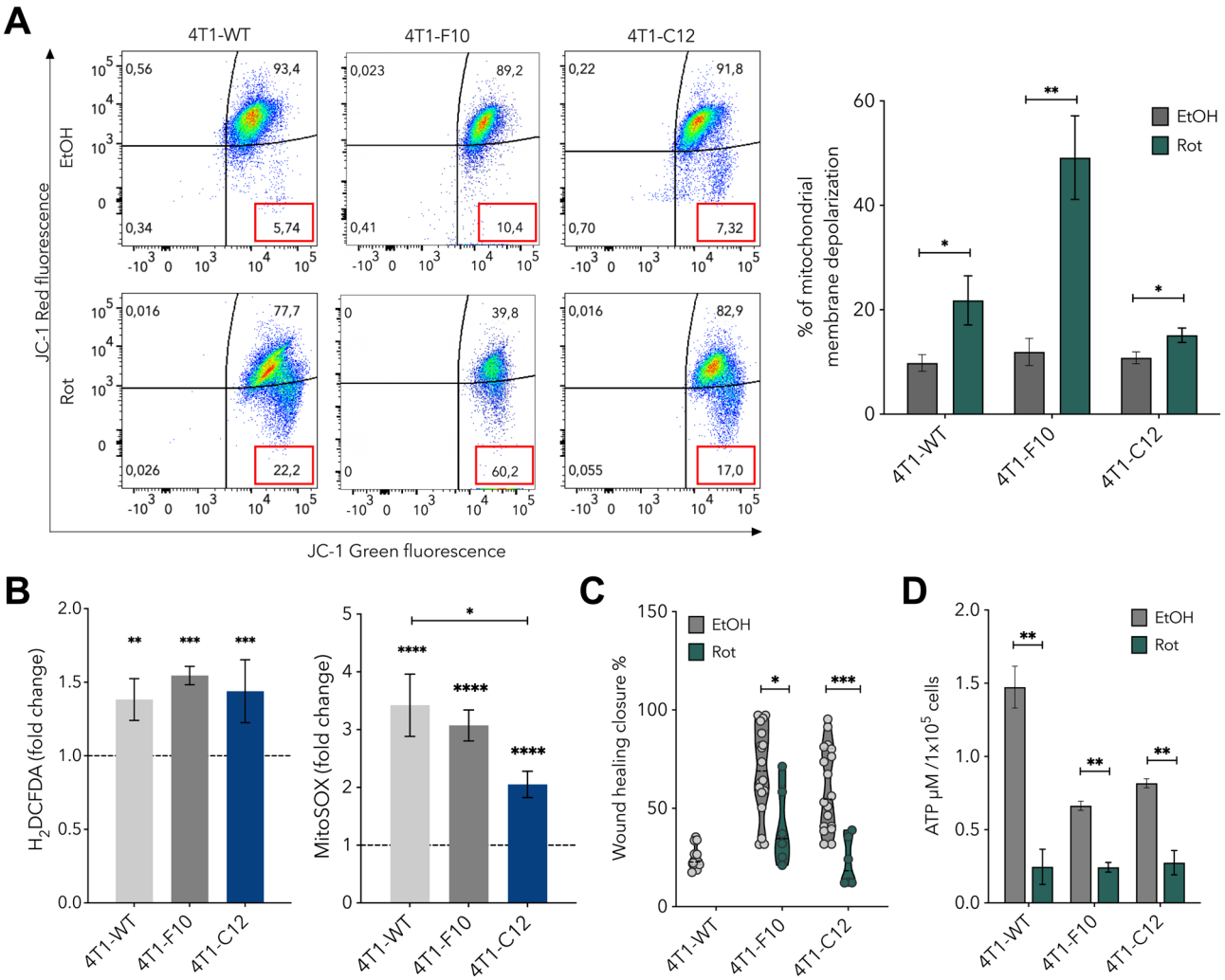

Fig. 4. Mitocans decrease migration in both clones. (**A**) JC-1 staining analysis was done in cells seeded overnight and treated with 1 µM of Rotenone for 24 h. Percentage of JC-1 aggregates expressed as mean ± SEM of three independent experiments is shown. (**B**) 4T1-WT, 4T1-F10 and 4T1-C12 clones were treated with 1 µM of Rotenone and after 24 h were stained with H_2DCFDA and MitoSOX showing MFI fold change compared with untreated cells (blue dot line). (**C**) 4T1-WT, 4T1-F10, and 4T1-C12 clones were treated with 0,1 µM rotenone for 48 h, percentage closure in 4T1-WT cells and clones is shown. (**D**) 4T1-WT, 4T1-F10, and 4T1-C12 clones were treated with 1 µM Rotenone, the graph shows the bioluminescence per 100.000 cells. Data are presented as the mean ± SEM of 3 independent experiments $^{*}p < 0.05$; $^{**}p < 0.01$; $^{***}p < 0.001$; $^{****}p < 0.0001$.

Anamu-SC generated a significant overall drop in OCR in 4T1-WT and their clones, with an increase in ECAR in the 4T1-C12 clone (Fig. 5E). Next, we examined how different treatments affected the induction of apoptosis and found that 4T1-C12 cells were more susceptible to apoptosis when exposed to Anamu-SC and rotenone than 4T1-WT and 4T1-F10 cells. P2Et did not trigger apoptosis in 4T1-F10 cells as effectively as it did in 4T1-WT cells (Fig. 5F and Fig. Suppl 1). We used the wound healing assay to determine how the extracts affected cell migration. We discovered that Anamu-SC treatment diminished migration in both clones, being significantly more robust in the clone with C1qbp inhibition and that outcomes are comparable with those with rotenone treatment (Fig. 5G). Instead, the P2Et therapy had no impact on the ability to migrate. These findings show that the C12 clone, which has a slightly lower mitochondrial mass and a reduced ECAR compared to 4T1-WT cells, it is more sensitive to mitocans like rotenone and Anamu-SC treatment, the latter of which also affects various metabolic features like glucose consumption, ATP production, as well as migration and apoptosis.

Anamu-SC treatment affects mitochondrial morphology

Considering that mitochondria is a molecular target of Anamu-SC[35], and that our current results seem to confirm this fact, we assessed whether there were changes in mitochondrial morphology. To test this, we treated WT cells and clones (F10 and C12) with Anamu-SC for 24 h and analyzed different factors related to mitochondria morphology, such as number (Nc), area (Am), mass, length (AR) and mitochondrial branching (FF) (Fig. 6A–C). Significant alterations were generated by Anamu-SC and rotenone treatments in the parameters as Nc, Am, mass

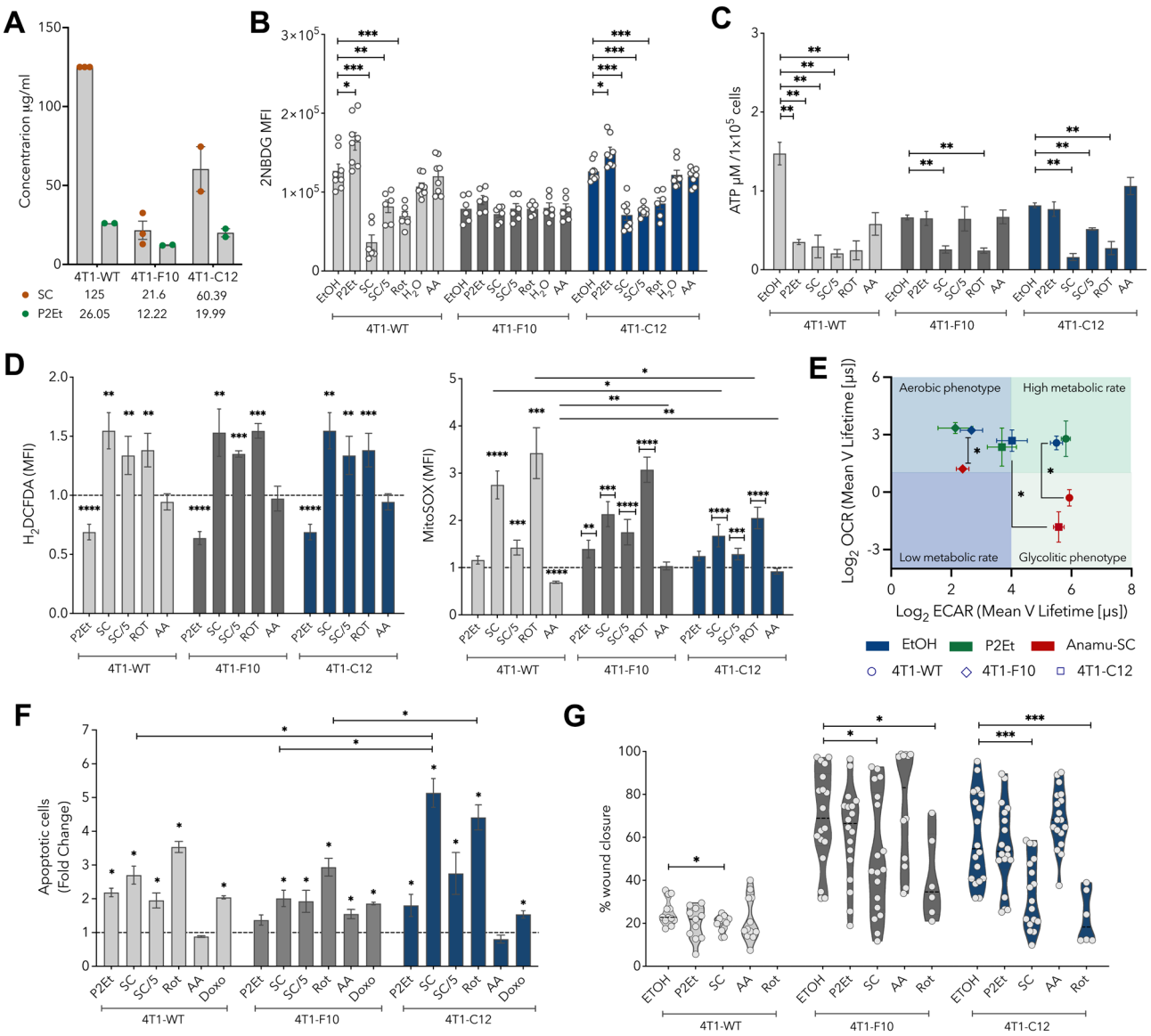

Fig. 5. Natural extracts with effect on metabolism reduce migration. (**A**) IC_{50} of P2Et and Anamu-SC treatment for each cell line, data were normalized to the viability of controls (EtOH-treated, vehicle). (**B**) 4T1-WT, 4T1-F10 and 4T1-C12 clones were treated with the IC_{50} of the natural extracts and controls for 24 h, then they were stained with 2NBDG dye showing MFI (median fluorescence intensity). (**C**) 4T1-WT, 4T1-F10 and 4T1-C12 clones were treated with the IC_{50} of the plants extracts and controls for 24 h, the graph shows the bioluminescence per 100.000 cells. (**D**) 4T1-WT, 4T1-F10 and 4T1-C12 clones were treated with the IC_{50} of the plants extracts and controls for 24 h, then they were stained with H_2DCFDA and MitoSOX Red (100 mM) showing MFI from each treatment relative to the vehicle for both dyes. (**E**) 30.000 cells were seeded of 4T1-WT cell line and their clones 4T1-F10 and 4T1-C12 in 96 well plate overnight, next day cells were treated with the IC_{50} of P2Et and Anamu-SC (SC) for 6 h and then the cells were stained with MitoXpress probe or pH-Xtra Glycolysis probe and OCR and ECAR were measured in Cytation 5. (**F**) 4T1-WT, 4T1-F10 and 4T1-C12 cells were treated with the IC_{50} of the plants extracts and controls for 24 h, a representative graph of percentage of apoptotic cells (sum of early and late apoptosis) is shown expressed as mean ± SEM for three independent experiments. (**G**) 4T1-WT, 4T1-F10 and 4T1-C12 clones were treated with 1/5 IC_{50} of P2Et and Anamu-SC (SC), Rotenone 0,1 µM and ascorbic acid (AA) 20 nM for 48 h and then performed cell migration assay (wound healing assay) and percentage closure in 4T1-WT cells and clones is shown. Data are presented as the mean ± SEM of 3 independent experiments $^{*}p<0.05$; $^{**}p<0.01$; $^{***}p<0.001$; $^{****}p<0.0001$.

(Fig. Suppl 2), mitochondrial length (Fig. 6B), and mitochondrial branching (Fig. 6C). In fact, all the parameters were reduced with Anamu-SC treatment in all the cells, in fact, we observed a more significant reduction on the 4T1-WT and the 4T1-C12 cells compared to the 4T1-F10 cells, however the Nc parameter and the mitochondrial mass tended to decrease in 4T1-C12 cells.

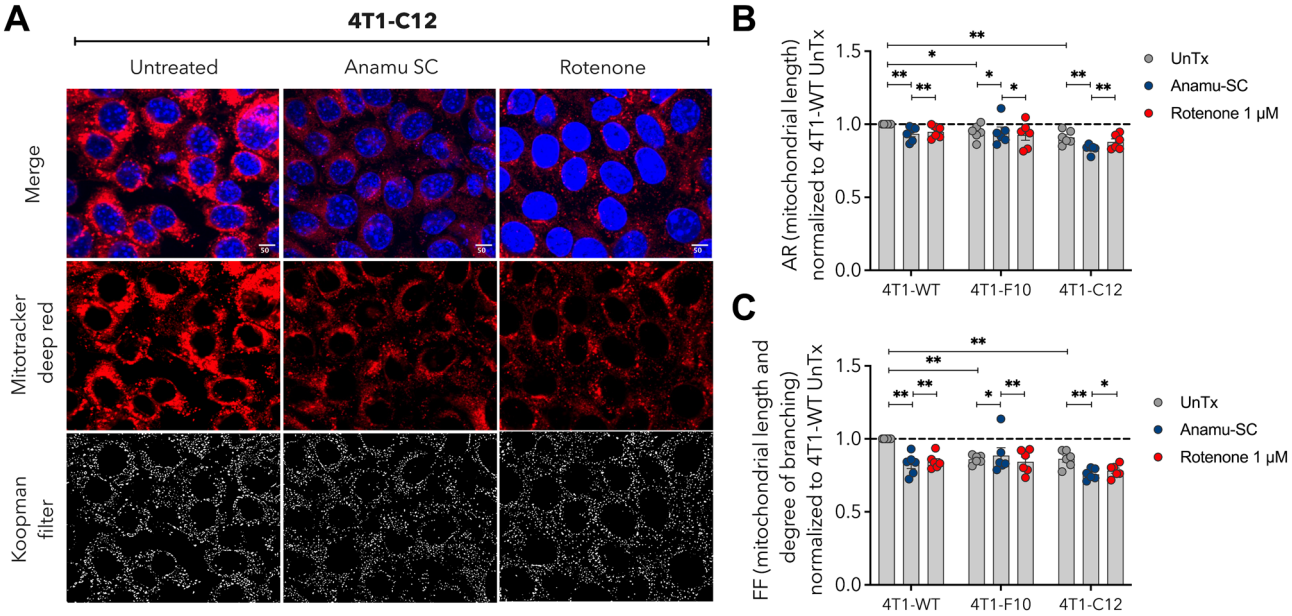

Fig. 6. Mitochondrial morphology is affected by Anamu-SC. (**A**) 4T1-WT, 4T1-F10 and 4T1-C12 clones were seeded overnight then were treated with Anamu-SC IC_{50} and rotenone 100 nM then were stained with Mitotracker deep red and DAPI (blue) for the nuclei. Images observed related to 4T1-C12 clone (merge, mitotracker deep red and Koopman filter). These images were acquired with confocal microscope Olympus FV1000 with an oil 60 × PlanAPO. Quantification of mitochondrial morphological changes, (**B**) length, and (**C**). mitochondrial branching in 4T1-WT, 4T1-F10, and 4T1-C12 treated with Anamu-SC and Rotenone for 24 h. Data are presented as the mean ± SEM of 2 independent experiments $^{*}p < 0.05$; $^{**}p < 0.01$; $^{***}p < 0.001$; $^{****}p < 0.0001$.

On the other hand, Rotenone reduced the Nc in all cell lines, however, the Am parameter was affected only on the 4T1-WT and 4T1-C12 cells; and the mitochondrial mass and FF were diminished in the 4T1-WT cells and both clones as Anamu-SC did. Here, the Anamu-SC showed a major impact on the mitochondrial network, leading to a reduction in branching as well as in mitochondrial length. These results suggest that the mitochondria is a target of Anamu-SC and therefore this could be proposed as a standardized polymolecular extract acting as a mitocan.

Discussion

Tumor metabolism represents a complex collection of metabolic changes that arise in response to genetic and nongenetic determinants. Metabolic reprogramming meets the demands of cell proliferation; however, there is a certain degree of heterogeneity given by the metabolic dependencies of any given tumor cell[5,67]. Due to the recognition of the complexity and metabolic heterogeneity, we designed two cellular models of triple-negative breast cancer with different metabolic requirements. Subsequently, we evaluated their biological behavior and response to metabolic modulators targeting the mitochondria. On one hand, we inhibited Hk-2 expression, an enzyme that regulates glycolysis, and on the other, we altered the gene expression of *C1qbp*, which codifies for a multifunctional chaperone-type protein in the mitochondria. We were able to show that the inhibition of Hk-2, clone 4T1-F10, makes cells more dependent on mitochondrial activity. Tumor mitochondrial metabolism has a vital role in metastatic triple-negative breast cancer. Even if this type of tumor relies on glycolysis, the OXPHOS is increased in metastatic tumors as well in chemo-resistant. In fact, OXPHOS inhibition in relapsed tumors reduced progression and improved the efficacy of chemotherapy, which suggests that targeting mitochondrial functions such as energy production by OXPHOS may be a novel approach to enhance the effectiveness of various targeted therapies for TNBC[31,68,69].

Indeed, due to the tumor's dependence on energy for the many stages of the metastatic process, such as detachment, extravasation, invasion, and new niche development, metabolism, and tumor migration are receiving more attention. Metastatic cells suffer a reprogramming of their metabolism, which results in increased OXPHOX activity in distant metastases[70]. Metastasis can occur in different ways in the primary tumor, mainly as individual or collective processes. In individual processes, an increase in mitochondrial metabolism is seen, bringing the mitochondria to the forefront, where they provide more ATP molecules to support migration. In the collective process, a heterogeneous population is composed of a leader cell and follower cells, which have a different metabolism compared to individual migration because the leader cell depends on glycolytic metabolism, which allows it to have ATP more quickly than the followers due to the high efficiency of glycolysis to generate ATP molecules from one molecule of glucose[71].

Besides, it has been demonstrated that natural compounds possess antimetastatic properties. In triple-negative breast cancer, apple polyphenol phloretin inhibits GLUT2 transporter, which suppresses the growth and metastasis of the malignancy[72]. Additionally, MC-4, an extract from *Artemisia annua L.*, decreased the growth of cancer

cells by suppressing the expression of GLUT1 and PKM2, key proteins on the glycolysis pathway. Furthermore, the combination with everolimus, an inhibitor of mTOR, reduced the metastatic process in advanced renal cell carcinoma[73]. Sulfur compounds are present in different natural extracts, as in the Anamu-SC extract presented here[34]; in fact, these organic sulfur compounds have shown epigenetic alterations that confer anticancer properties; also, different pathways where these sulfurs have an effect in cancer, such as a reduction in metastasis, a disruption in the cell cycle, and, inhibition in proliferation, among others, have been published[74].

Although the mechanisms of migration and invasiveness are not yet well understood, the link between metabolism and migration has led to the active search for molecules that affect mitochondria (mitogens)[26]. Targeting processes such as ETC by inhibiting complex I induce cytotoxicity and increased sensitivity to chemotherapy, as was demonstrated in pancreatic cancer[75]. Equally important has been the mitochondrial dynamic study; in TNBC, mitochondria are smaller and fragmented than in non-triple negative breast cancers correlating with poor prognosis. Therefore, the focus of interest is to search for molecules that inhibit fission[69]; however, until now, there are no recognized molecules for this purpose.

The complex processes of mitochondrial activity greatly influence tumor cells' behavior, survival, and growth. Our study demonstrates that Anamu-SC extract can modify metabolism by reducing cellular respiration and mitochondrial biogenesis and affecting mitochondrial morphology in breast cancer cells. These changes could explain its ability to decrease cell migration and its cytotoxic effect in cancer, suggesting that it acts as a "mitocan". On the contrary, P2Et extract does not result in appreciable changes to mitochondrial shape or metabolism. However, P2Et affected cellular respiration in a leukemia model but not mitochondrial morphology (unpublished data). Previous research on the B16 melanoma model showed that P2Et triggers the activation of the endoplasmic reticulum stress response, leading to the intracellular release of calcium, and potentially inducing the generation of markers associated with immunogenic cell death[32]; these results suggest that while both extracts exhibit anticancer effects they operate through distinct mechanisms, having Anamu-SC playing a significant capacity to interfere tumor metabolism and mitochondrial function.

Other authors have shown how natural products influence the migration of tumor cells through mechanisms distinct from those that are metabolic-related. Ferulic acid and coumarin derivatives can alter melatonin receptors, which generates an anti-migratory and antiproliferative effect on different breast cancer cell lines, and particularly curcumin can intervene in PI3K/Akt signaling, preventing cell migration of the MDA-MB-231 line[76,77]. In turn, Cordycepin, a nucleoside isolated from *Cordyceps*, negatively regulates mitochondrial function and limits energy production, leading to inhibition of metastasis and migration in ovarian cancer[78,79]. Also, lupeol, a pentacyclic triterpenoid compound, induces mitochondrial hyper-fission, eventually leading to apoptosis in renal carcinoma cells[80].

In conclusion, we introduce a mouse model of triple-negative breast cancer (TNBC) where the tumor cell´s energy metabolism was modulated by the anti-tumor effect of two distinct plant extracts. The first, P2Et, known for its significant antitumor effect in melanoma, and leukemia models[32,33,45,81–83], appears to have no impact on the metabolic pathways in this TNBC model. On the other hand, Anamu-SC, primarily focuses on targeting mitochondria, while also impacting various metabolic aspects, particularly the reduction in oxygen consumption rate (OCR), besides, it has been found with other extracts derived from *P. alliacea* the capacity to reduce respiration and disrupt vital metabolic pathways involved in the proliferation of leukemic cells[49]. This leads to an enhancement of the cytotoxic capabilities and a decrease in the migration ability, which could be principally beneficial in metastatic cells. Therefore, we propose the Anamu-SC plant extract as a promising mitocan.

Data availability

The authors declare that the data supporting the findings of this study are available within the paper and its Supplementary Information files. Should any raw data files be needed in another format, they are available from the corresponding author upon reasonable request.

Received: 19 July 2024; Accepted: 19 August 2024
Published online: 31 August 2024

References

1. Warburg, O. The metabolism of tumors in the body. *J. Gen. Physiol.* **8**, 519–530 (1927).
2. Solaini, G., Sgarbi, G. & Baracca, A. Oxidative phosphorylation in cancer cells. *Biochim. Biophys. Acta (BBA)-Bioenerg.* **1807**, 534–542 (2011).
3. Hanahan, D. & Weinberg, R. A. Hallmarks of cancer: The next generation. *Cell* **144**, 646–674 (2011).
4. Hanahan, D. Hallmarks of cancer: New dimensions. *Cancer Discov.* **12**, 31–46 (2022).
5. Martínez-Reyes, I. & Chandel, N. S. Cancer metabolism: Looking forward. *Nat. Rev. Cancer* **21**, 669–680 (2021).
6. van Niekerk, G. & Engelbrecht, A.-M. Role of PKM2 in directing the metabolic fate of glucose in cancer: A potential therapeutic target. *Cell. Oncol.* **41**, 343–351 (2018).
7. Shiratori, R. *et al.* Glycolytic suppression dramatically changes the intracellular metabolic profile of multiple cancer cell lines in a mitochondrial metabolism-dependent manner. *Sci. Rep.* **9**, 18699 (2019).
8. Mathupala, S. P., Ko, Y. H. & Pedersen, P. L. Hexokinase II: Cancer's double-edged sword acting as both facilitator and gatekeeper of malignancy when bound to mitochondria. *Oncogene* **25**, 4777–4786 (2006).
9. DeWaal, D. *et al.* Hexokinase-2 depletion inhibits glycolysis and induces oxidative phosphorylation in hepatocellular carcinoma and sensitizes to metformin. *Nat. Commun.* **9**, 446 (2018).
10. Patra, K. C. *et al.* Hexokinase 2 is required for tumor initiation and maintenance and its systemic deletion is therapeutic in mouse models of cancer. *Cancer Cell* **24**, 213–228 (2013).
11. Fogal, V. *et al.* Mitochondrial p32 protein is a critical regulator of tumor metabolism via maintenance of oxidative phosphorylation. *Mol. Cell Biol.* **30**, 1303–1318 (2010).
12. Gotoh, K. *et al.* Mitochondrial p32/C1qbp is a critical regulator of dendritic cell metabolism and maturation. *Cell Rep.* **25**, 1800-1815.e4 (2018).

13. Gong, Y. *et al.* Metabolic-pathway-based subtyping of triple-negative breast cancer reveals potential therapeutic targets. *Cell Metab.* **33**, 51-64.e9 (2021).
14. Wang, Z., Jiang, Q. & Dong, C. Metabolic reprogramming in triple-negative breast cancer. *Cancer Biol. Med.* **17**, 44–59 (2020).
15 Sun, X. *et al.* Metabolic reprogramming in triple-negative breast cancer. *Front. Oncol.* **10**, 428 (2020).
16. Yin, L., Duan, J.-J., Bian, X.-W. & Yu, S. Triple-negative breast cancer molecular subtyping and treatment progress. *Breast Cancer Res.* **22**, 61 (2020).
17. Li, Y. *et al.* Recent advances in therapeutic strategies for triple-negative breast cancer. *J. Hematol. Oncol.* **15**, 121 (2022).
18. Baranova, A. *et al.* Triple-negative breast cancer: Current treatment strategies and factors of negative prognosis. *J. Med. Life* **15**, 153–161 (2022).
19. Liao, H., Wang, Z., Deng, Z., Ren, H. & Li, X. Curcumin inhibits lung cancer invasion and metastasis by attenuating GLUT1/MT1-MMP/MMP2 pathway. *Int. J. Clin. Exp. Med.* **8**(6), 8948 (2015).
20. Vaughan, R. A. *et al.* Tumor necrosis factor alpha induces Warburg-like metabolism and is reversed by anti-inflammatory curcumin in breast epithelial cells. *Int. J. Cancer* **133**, 2504–2510 (2013).
21. Brito, A. F. *et al.* New approach for treatment of primary liver tumors: The role of quercetin. *Nutr. Cancer* **68**, 250–266 (2016).
22 Zhao, Y., Chard Dunmall, L. S., Cheng, Z., Wang, Y. & Si, L. Natural products targeting glycolysis in cancer. *Front. Pharmacol.* **13**, 1036502 (2022).
23 Cui, Y. *et al.* Natural products targeting glycolytic signaling pathways-an updated review on anti-cancer therapy. *Front. Pharmacol.* **13**, 1035882 (2022).
24. Mani, S., Swargiary, G. & Singh, K. K. Natural agents targeting mitochondria in cancer. *Int. J. Mol. Sci.* **21**, 6992 (2020).
25. Vasan, K., Werner, M. & Chandel, N. S. Mitochondrial metabolism as a target for cancer therapy. *Cell Metab.* **32**, 341–352 (2020).
26. Dong, L., Gopalan, V., Holland, O. & Neuzil, J. Mitocans revisited: Mitochondrial targeting as efficient anti-cancer therapy. *Int. J. Mol. Sci.* **21**, 7941 (2020).
27 Gao, F. *et al.* Epigallocatechin gallate inhibits human tongue carcinoma cells via HK2-mediated glycolysis. *Oncol. Rep.* **33**, 1533–1539 (2015).
28. Sánchez-Tena, S., Alcarraz-Vizán, G., Marín, S., Torres, J. L. & Cascante, M. Epicatechin gallate impairs colon cancer cell metabolic productivity. *J. Agric. Food Chem.* **61**, 4310–4317 (2013).
29. Yang, Y., He, P.-Y., Zhang, Y. & Li, N. Natural products targeting the mitochondria in cancers. *Molecules* **26**, 92 (2020).
30. Chen, V. *et al.* Bezielle selectively targets mitochondria of cancer cells to inhibit glycolysis and OXPHOS. *PLoS One* **7**, e30300 (2012).
31. Evans, K. W. *et al.* Oxidative phosphorylation is a metabolic vulnerability in chemotherapy-resistant triple-negative breast cancer. *Cancer Res.* **81**, 5572–5581 (2021).
32. Prieto, K. *et al.* Polyphenol-rich extract induces apoptosis with immunogenic markers in melanoma cells through the ER stress-associated kinase PERK. *Cell Death Discov.* **5**, 134 (2019).
33. Gomez-Cadena, A. *et al.* Immune-system-dependent anti-tumor activity of a plant-derived polyphenol rich fraction in a melanoma mouse model. *Cell Death Dis.* **7**, e2243–e2243 (2016).
34. Ballesteros-Ramírez, R. *et al.* Preferential activity of *Petiveria alliacea* extract on primary myeloid leukemic blast. *Evid. Based Complement. Altern. Med.* **2020**, 1–14 (2020).
35. Hernández, J. F. *et al.* A cytotoxic *Petiveria alliacea* dry extract induces ATP depletion and decreases β-F1-ATPase expression in breast cancer cells and promotes survival in tumor-bearing mice. *Rev. Bras. Farmacogn.* **27**, 306–314 (2017).
36. Chinnikrishnan, P. *et al.* The role of selective flavonoids on triple-negative breast cancer: An update. *Separations* **10**, 207 (2023).
37. Urueña, C. *et al. Petiveria alliacea* extracts uses multiple mechanisms to inhibit growth of human and mouse tumoral cells. *BMC Complement. Altern. Med.* **8**, 60 (2008).
38. Hernandez, J. F. *et al.* A *Petiveria alliacea* standardized fraction induces breast adenocarcinoma cell death by modulating glycolytic metabolism. *J. Ethnopharmacol.* **153**, 641–649 (2014).
39 Sandoval, T. *et al.* Standarized extract from *Caesalpinia spinosa* is cytotoxic over cancer stem cells and enhance anticancer activity of doxorubicin. *Am. J. Chin. Med.* **44**, 1693–1717 (2016).
40. Castaneda, D. M., Pombo, L. M., Uruena, C. P., Hernandez, J. F. & Fiorentino, S. A gallotannin-rich fraction from *Caesalpinia spinosa* (Molina) Kuntze displays cytotoxic activity and raises sensitivity to doxorubicin in a leukemia cell line. *BMC Complement. Altern. Med* **12**, 38 (2012).
41. Urueña, C. *et al.* Gallotannin-rich *Caesalpinia spinosa* fraction decreases the primary tumor and factors associated with poor prognosis in a murine breast cancer model. *BMC Complement. Altern. Med.* **13**, 74 (2013).
42. Lasso, P. *et al.* Natural products induce different anti-tumor immune responses in murine models of 4T1 mammary carcinoma and B16-F10 melanoma. *Int. J. Mol. Sci.* **24**, 16698 (2023).
43. Jiménez, M. C. *et al.* Plant extract from *Caesalpinia spinosa* inhibits cancer-associated fibroblast-like cells generation and function in a tumor microenvironment model. *Heliyon* **9**, e14148 (2023).
44. Urueña, C. *et al.* Multifunctional T lymphocytes generated after therapy with an antitumor gallotanin-rich normalized fraction are related to primary tumor size reduction in a breast cancer model. *Integr. Cancer Ther.* **14**, 468–483 (2015).
45. Lasso, P. *et al.* Breast tumor cells highly resistant to drugs are controlled only by the immune response induced in an immunocompetent mouse model. *Integr. Cancer Ther.* **18**, 1534735419848047 (2019).
46. Elisseeva, S., Santovito, E., Linehan, E., Kerry, J. P. & Papkovsky, D. B. Performance assessment of the two oxygen sensor based respirometric platforms with complex media and in selective bacterial assays. *Sens. Actuators B Chem.* **383**, 133582 (2023).
47. Alderman, J. *et al.* A low-volume platform for cell-respirometric screening based on quenched-luminescence oxygen sensing. *Biosens. Bioelectron.* **19**, 1529–1535 (2004).
48. Hynes, J. *et al.* A high-throughput dual parameter assay for assessing drug-induced mitochondrial dysfunction provides additional predictivity over two established mitochondrial toxicity assays. *Toxicol. in Vitro* **27**, 560–569 (2013).
49. Rojas, L. *et al.* Effect of *Petiveria alliacea* extracts on metabolism of K562 myeloid leukemia cells. *Int. J. Mol. Sci.* **24**, 17418 (2023).
50 Sinclair, L. V., Barthelemy, C. & Cantrell, D. A. Single cell glucose uptake assays: A cautionary tale. *Immunometabolism* **2**, e200029 (2020).
51. Zou, C., Wang, Y. & Shen, Z. 2-NBDG as a fluorescent indicator for direct glucose uptake measurement. *J. Biochem. Biophys. Methods* **64**, 207–215 (2005).
52. Lasso, P. *et al.* Piper nigrum extract suppresses tumor growth and enhances the antitumor immune response in murine models of breast cancer and melanoma. *Cancer Immunol. Immunother.* **72**, 3279–3292 (2023).
53. Lasso, P. *et al.* Tillandsia usneoides extract decreases the primary tumor in a murine breast cancer model but not in melanoma. *Cancers (Basel)* **14**, 5383 (2022).
54. Koopman, G. *et al.* Annexin V for flow cytometric detection of phosphatidylserine expression on B cells undergoing apoptosis. *Blood* **84**, 1415–1420 (1994).
55. Vermes, I., Haanen, C., Steffens-Nakken, H. & Reutellingsperger, C. A novel assay for apoptosis flow cytometric detection of phosphatidylserine expression on early apoptotic cells using fluorescein labelled Annexin V. *J. Immunol. Methods* **184**, 39–51 (1995).
56. Koopman, W. J. H., Visch, H., Smeitink, J. A. M. & Willems, P. H. G. M. Simultaneous quantitative measurement and automated analysis of mitochondrial morphology, mass, potential, and motility in living human skin fibroblasts. *Cytom. Part A* **69A**, 1–12 (2006).

57. Tronstad, K. *et al.* Regulation and quantification of cellular mitochondrial morphology and content. *Curr. Pharm. Des.* **20**, 5634–5652 (2014).
58. Jonkman, J. E. N. *et al.* An introduction to the wound healing assay using live-cell microscopy. *Cell Adhes. Migr.* **8**, 440–451 (2014).
59. Radstake, W. E. *et al.* Comparison of in vitro scratch wound assay experimental procedures. *Biochem. Biophys. Rep.* **33**, 101423 (2023).
60. Mego, M. *et al.* Expression of epithelial–mesenchymal transition-inducing transcription factors in primary breast cancer: The effect of neoadjuvant therapy. *Int. J. Cancer* **130**, 808–816 (2012).
61. Simões, R. V. *et al.* Metabolic plasticity of metastatic breast cancer cells: Adaptation to changes in the microenvironment. *Neoplasia* **17**, 671–684 (2015).
62. Lanning, N. J. *et al.* Metabolic profiling of triple-negative breast cancer cells reveals metabolic vulnerabilities. *Cancer Metab.* **5**, 6 (2017).
63. Sciacovelli, M. & Frezza, C. Metabolic reprogramming and epithelial-to-mesenchymal transition in cancer. *FEBS J.* **284**, 3132–3144 (2017).
64 Georgakopoulos-Soares, I., Chartoumpekis, D. V., Kyriazopoulou, V. & Zaravinos, A. EMT factors and metabolic pathways in cancer. *Front. Oncol.* **10**, 499 (2020).
65. Jia, D. *et al.* Towards decoding the coupled decision-making of metabolism and epithelial-to-mesenchymal transition in cancer. *Br. J. Cancer* **124**, 1902–1911 (2021).
66. Panda, V., Khambat, P. & Patil, S. Mitocans as novel agents for anticancer therapy: An overview. *Int. J. Clin. Med.* **02**, 515–529 (2011).
67 Loponte, S., Lovisa, S., Deem, A. K., Carugo, A. & Viale, A. The many facets of tumor heterogeneity: Is metabolism lagging behind?. *Cancers (Basel)* **11**, 1574 (2019).
68. Baek, M. L. *et al.* Mitochondrial structure and function adaptation in residual triple negative breast cancer cells surviving chemotherapy treatment. *Oncogene* **42**, 1117–1131 (2023).
69 Weiner-Gorzel, K. & Murphy, M. Mitochondrial dynamics, a new therapeutic target for triple negative breast cancer. *Biochim. Biophys. Acta (BBA)-Rev. Cancer* **1875**, 188518 (2021).
70. Ganguly, K. & Kimmelman, A. C. Reprogramming of tissue metabolism during cancer metastasis. *Trends Cancer* **9**, 461–471 (2023).
71. Zhang, J. *et al.* Energetic regulation of coordinated leader–follower dynamics during collective invasion of breast cancer cells. *Proc. Natl. Acad. Sci.* **116**, 7867–7872 (2019).
72. Wu, K.-H. *et al.* The apple polyphenol phloretin inhibits breast cancer cell migration and proliferation via inhibition of signals by type 2 glucose transporter. *J. Food Drug Anal.* **26**, 221–231 (2018).
73. Son, J. Y. *et al.* Novel therapeutic roles of MC-4 in combination with everolimus against advanced renal cell carcinoma by dual targeting of Akt/pyruvate kinase muscle isozyme M2 and mechanistic target of rapamycin complex 1 pathways. *Cancer Med.* **7**, 5083–5095 (2018).
74 Shoaib, S. *et al.* Prospective epigenetic actions of organo-sulfur compounds against cancer: Perspectives and molecular mechanisms. *Cancers (Basel)* **15**, 697 (2023).
75. Boukalova, S. *et al.* Mitochondrial targeting of metformin enhances its activity against pancreatic cancer. *Mol. Cancer Ther.* **15**, 2875–2886 (2016).
76. Guan, F. *et al.* Curcumin suppresses proliferation and migration of MDA-MB-231 breast cancer cells through autophagy-dependent Akt degradation. *PLoS One* **11**, e0146553 (2016).
77. Hasan, M., Genovese, S., Fiorito, S., Epifano, F. & Witt-Enderby, P. A. Oxyprenylated phenylpropanoids bind to MT1 melatonin receptors and inhibit breast cancer cell proliferation and migration. *J. Nat. Prod.* **80**, 3324–3329 (2017).
78. Wang, X.-A. *et al.* Cordycepin induces S phase arrest and apoptosis in human gallbladder cancer cells. *Molecules* **19**, 11350–11365 (2014).
79. Wang, C.-W., Hsu, W.-H. & Tai, C.-J. Antimetastatic effects of cordycepin mediated by the inhibition of mitochondrial activity and estrogen-related receptor α in human ovarian carcinoma cells. *Oncotarget* **8**, 3049–3058 (2017).
80. Sinha, K. *et al.* Lupeol alters viability of SK-RC-45 (Renal cell carcinoma cell line) by modulating its mitochondrial dynamics. *Heliyon* **5**, e02107 (2019).
81. Alejandra, G. -C. Adaptive immune system dependent anti-tumor activity of a polyphenol rich fraction from *Caesalpinia spinosa* in the B16 melanoma mouse model. *Cell Death Dis* **7**, e2243 (2016).
82. Corzo Prada, L. *et al.* Doxorubicin activity is modulated by traditional herbal extracts in a 2D and 3D multicellular sphere model of leukemia. *Pharmaceutics* **15**, 1690 (2023).
83 Arévalo, C. M., Cruz-Rodriguez, N., Quijano, S. & Fiorentino, S. Plant-derived extracts and metabolic modulation in leukemia: A promising approach to overcome treatment resistance. *Front. Mol. Biosci.* **10**, 1229760 (2023).

Acknowledgements

The authors would like to thank Pontificia Universidad Javeriana and the Colombian Environmental Ministry for allowing the use of genetic resources through the Contract of Access to Genetic Resources No. 220 of 2018 for Colombian plant material.

Author contributions

Conceptualization C.C., S.F and A.B.; conducted experiments M.C.J., C.A., and C.C.; data collection and data analysis M.C.J., C.A., P.L., C.U and C.C.; data interpretation C.A., P.L., C.C., and A.B.; manuscript writing C.C., and A.B.; writing review and critical revision M.C.J., C.A., P.L., C.U., C.C., A.B., and S.F. Grant acquisitions S.F and AB. All authors have read and agreed to the published version of the manuscript.

Funding

This project was funded by Pontificia Universidad Javeriana, Ministerio de Ciencia, Tecnología e Innovación, Ministerio de Educación Nacional, Ministerio de Industria, Comercio y Turismo and ICETEX, 2ª Convocatoria Ecosistema Científico–Colombia Científica 792–2017, Program "Generación de alternativas terapéuticas en cáncer a partir de plantas a través de procesos de investigación y desarrollo traslacional, articulados en sistemas de valor sostenibles ambiental y económicamente" (Contract no. FP44842-221–2018). We thank the Vicerrectoria de Investigaciones at the Pontificia Universidad Javeriana for the financial support to publish this research (Proposal ID 00010639).

Competing interests

S.F. and C.U. are inventors of a granted patent related to P2Et. SF and CU are partners of the DreemBio company who was a licensee of related patents. The rest of the authors declare no competing interests.

Additional information

Supplementary Information The online version contains supplementary material available at https://doi.org/10.1038/s41598-024-70550-z.

Correspondence and requests for materials should be addressed to A.B.

Reprints and permissions information is available at www.nature.com/reprints.

Publisher's note Springer Nature remains neutral with regard to jurisdictional claims in published maps and institutional affiliations.